



**Murdoch**  
UNIVERSITY

## MURDOCH RESEARCH REPOSITORY

*This is the author's final version of the work, as accepted for publication following peer review but without the publisher's layout or pagination.*

*The definitive version is available at*

<http://dx.doi.org/10.1016/j.electacta.2010.09.011>

**Minakshi, M. (2010) *Lithium intercalation into amorphous FePO<sub>4</sub> cathode in aqueous solutions*. *Electrochimica Acta*, 55 (28). pp. 9174-9178.**

<http://researchrepository.murdoch.edu.au/3352/>

Copyright: © 2010 Elsevier Ltd  
It is posted here for your personal use. No further distribution is permitted.

## Accepted Manuscript

Title: Lithium Intercalation into Amorphous FePO<sub>4</sub> Cathode in Aqueous Solutions

Author: Manickam Minakshi

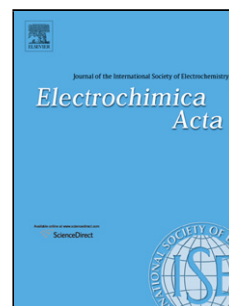
PII: S0013-4686(10)01170-9  
DOI: doi:10.1016/j.electacta.2010.09.011  
Reference: EA 16153

To appear in: *Electrochimica Acta*

Received date: 28-7-2010  
Revised date: 5-9-2010  
Accepted date: 5-9-2010

Please cite this article as: M. Minakshi, Lithium Intercalation into Amorphous FePO<sub>4</sub> Cathode in Aqueous Solutions, *Electrochimica Acta* (2010), doi:10.1016/j.electacta.2010.09.011

This is a PDF file of an unedited manuscript that has been accepted for publication. As a service to our customers we are providing this early version of the manuscript. The manuscript will undergo copyediting, typesetting, and review of the resulting proof before it is published in its final form. Please note that during the production process errors may be discovered which could affect the content, and all legal disclaimers that apply to the journal pertain.



# Lithium Intercalation into Amorphous FePO<sub>4</sub> Cathode in Aqueous Solutions

**Manickam Minakshi**

Faculty of Minerals and Energy, Murdoch University, Murdoch, WA 6150, Australia

## Abstract

Amorphous iron phosphate (FePO<sub>4</sub>) was investigated as a cathode material for battery applications using aqueous (lithium hydroxide or potassium hydroxide) electrolytes. Phosphate-based cathode materials are of great interest in lithium batteries which use non-aqueous electrolytes. In order for these materials to be used as cathodes in aqueous electrolytes it is important to understand their reduction/oxidation mechanisms. Potentiostatic and galvanostatic techniques are used to study these mechanisms. X-ray diffraction (XRD), Scanning electron microscopy (SEM) and X-ray photoelectron spectroscopy (XPS) have been used to gain insight into the reduction/oxidation behavior of FePO<sub>4</sub> cathodes. Our results show that FePO<sub>4</sub> undergoes reversible Fe<sup>3+/2+</sup> processes of reduction and oxidation in LiOH electrolyte, while using KOH electrolyte this process is found to be irreversible. The lithium intercalation mechanism is identified for LiOH while in the case of KOH electrolyte H reacts to form FeOOH. The Zn|LiOH|FePO<sub>4</sub> battery provides a reversible capacity of 65 mAh/g. The results indicate the trigonal FePO<sub>4</sub> as an attractive host intercalation compound.

**Keywords:** Iron phosphate, rechargeable, battery, aqueous, trigonal.

\* Corresponding author

Tel.: +61-8-9360-6784. Fax: +61-8-9310-1711. E-mail: [minakshi@murdoch.edu.au](mailto:minakshi@murdoch.edu.au); [lithiumbattery@hotmail.com](mailto:lithiumbattery@hotmail.com)

## 1. Introduction

1  
2 The cathode material of a rechargeable battery is a host insertion compound  
3  
4 into/from which any alkali cations can be reversibly inserted/extracted over a  
5  
6 compositional range during redox reactions [1]. The possible cathode materials  
7  
8 providing good rechargeability are layered  $\text{LiCoO}_2$ ,  $\text{LiNiO}_2$  and spinel  $\text{LiMn}_2\text{O}_4$ . The  
9  
10 use of  $\text{LiMn}_2\text{O}_4$  alleviates the problems associated with Co and Ni toxicity and its  
11  
12 cost, but the major issue hindering the development of this material is the loss of  
13  
14 capacity with extensive cycling, particularly at elevated temperatures [2].  
15  
16  
17  
18

19 Following the oxide-based materials, a technological breakthrough occurred  
20  
21 with the use of phosphates as cathodes in rechargeable non-aqueous lithium batteries.  
22  
23 The cathode performance of a lithium iron phosphate ( $\text{LiFePO}_4$ ) adopting an ordered  
24  
25 olivine structure was first reported by Padhi et al. [3] who proposed  $\text{LiFePO}_4$  as a  
26  
27 potential cathode in non-aqueous batteries. Subsequently, extensive work on this  
28  
29 material has been carried out by a number of researchers [4–8] and  $\text{LiFePO}_4$  is now  
30  
31 recognised as the active cathode for a new generation of lithium batteries. This is due  
32  
33 to its low cost, environmentally-friendly properties and good rechargeability. The  
34  
35 trigonal iron phosphate (analog of olivine) consists of corner shared framework with  
36  
37 the  $\text{FeO}_4$  and  $\text{PO}_4$  tetrahedra. The only difference between trigonal and olivine  
38  
39 structure is that of  $\text{FeO}_4$  tetrahedra instead of the  $\text{FeO}_6$  octahedra share common  
40  
41 corners.  $\text{FePO}_4$  has a potential application for an intercalation host compound [9].  
42  
43  
44  
45  
46  
47  
48

49 The mechanism through which  $\text{LiFePO}_4$  undergoes reduction/oxidation  
50  
51 reactions in non-aqueous lithium battery has been widely discussed in the literature  
52  
53 [10–13]. The focus of this paper is to investigate  $\text{FePO}_4$  for use with aqueous  
54  
55 electrolytes. The current work follows our extensive research on  $\text{MnO}_2$  [14] in  
56  
57 aqueous solution where we reported that the reduction mechanism involves both  
58  
59  
60  
61  
62  
63  
64  
65

1  
2  
3  
4  
5  
6  
7  
8  
9  
10  
11  
12  
13  
14  
15  
16  
17  
18  
19  
20  
21  
22  
23  
24  
25  
26  
27  
28  
29  
30  
31  
32  
33  
34  
35  
36  
37  
38  
39  
40  
41  
42  
43  
44  
45  
46  
47  
48  
49  
50  
51  
52  
53  
54  
55  
56  
57  
58  
59  
60  
61  
62  
63  
64  
65

lithium ( $\text{Li}^+$ ) and proton ( $\text{H}^+$ ) intercalation, but protons cannot de-intercalate reversibly. However, incorporation of additives [15–16] into  $\text{MnO}_2$  leads to improved electrochemical performance while preventing the formation of non-rechargeable products. This has motivated the search for new cathode materials suitable for aqueous rechargeable batteries.

Here, we report on the electrochemical performance of trigonal  $\text{FePO}_4$  as a cathode material in a rechargeable cell based on  $\text{LiOH}$  or  $\text{KOH}$  electrolytes.  $\text{Zn}$  metal is chosen as anode material. The use of trigonal  $\text{FePO}_4$  in a non-aqueous lithium battery was reported by Okada et al. [17] whereas its application in a cell with aqueous  $\text{LiOH}$  and  $\text{KOH}$  solution is reported here for the first time.

## 2. Experimental

### 2.1 Synthesis

The amorphous iron phosphate ( $\text{FePO}_4$ ) material used in this work was synthesized by a simple and inexpensive method identical to that described by Okada et al. [17]. The stoichiometric ratios of starting materials such as metallic iron and  $\text{P}_2\text{O}_5$  were mixed in ethanol for an hour in an agate mortar. The slurry was evaporated at  $90\text{ }^\circ\text{C}$  for 30 min and the resultant precursor was fine ground and calcined at  $200\text{ }^\circ\text{C}$  for 12 h to yield the amorphous  $\text{FePO}_4$  material. The  $\text{Fe}^{3+/2+}$  redox couple in the amorphous iron phosphate is reported [17] to be fully reversible than the crystalline counterpart. The crystalline  $\text{FePO}_4$  phase is known to be electrochemically inactive [18]. Hence, in this work, synthesis temperature is chosen to be  $200\text{ }^\circ\text{C}$ .

### 2.2 Material Characterization

The products formed during the cathodic and anodic scan were characterized by X-ray diffraction (XRD), X-ray photoelectron spectroscopy (XPS) and Scanning electron microscopy (SEM). For XRD analysis, X-ray diffractometer (Siemens) using  $\text{Cu-K}\alpha$

1 radiation was used. XPS (Kratos Ultra Axis Spectrometer) using monochromatic Al  
2  $K\alpha$  (1486.6 eV) radiation was used to analyze the chemical binding energies of the  
3 samples. XPS analysis was started when the pressure in the analysis chamber fell  
4 below  $1 \times 10^{-9}$  hPa. Carbon, C (1s), was used as a reference for all samples. A SEM  
5 (Philips Analytical XL series 20) was used for surface analysis investigations.  
6  
7  
8  
9

### 10 **2.3 Potentiostatic measurements: Slow-scan cyclic voltammetry**

11 For cyclic voltammetry (CV) experiments, a three-electrode cell was used. The  
12 working electrode was disk-shaped (10 mm diameter with 1 mm thickness)  $\text{FePO}_4$ .  
13 This disk was embedded in Pt gauze through which the electrical contact was made.  
14 On the other side of the disk, a layer of carbon was also pressed. The disk was  
15 inserted in a Teflon barrel on top of the carbon side and electrical contact was made  
16 by means of a brass plunger. The working  $\text{FePO}_4$  surface was exposed to electrolyte  
17 through a hole of 1 mm in the Teflon barrel. The counter-electrode was strip of Zn  
18 foil, separated from the main electrolyte by means of a porous frit. Hg/HgO served as  
19 the reference electrode. The electrolyte was a 5 M of either lithium hydroxide or  
20 potassium hydroxide. The working electrode was cycled between 0.2 to  $-0.4$  V at 25  
21  $\mu\text{V/s}$  scan rate. On each occasion, the potential scan started at 0.2 V, moving initially  
22 in the cathodic direction. At the reduction and oxidation points of the experiment, the  
23 cathode material was removed from the solution, washed with water and characterized  
24 by XRD, XPS and SEM analysis. All the cyclic voltammetry experiments were done  
25 using an EG & G Princeton Applied Research Versa Stat III model. All potentials  
26 were measured relative to the Hg/HgO electrode. All the electrochemical  
27 measurements were carried out in an ambient room atmosphere ( $25 \pm 1^\circ \text{C}$ ).  
28  
29  
30  
31  
32  
33  
34  
35  
36  
37  
38  
39  
40  
41  
42  
43  
44  
45  
46  
47  
48  
49  
50  
51  
52  
53  
54  
55

### 56 **2.4 Galvanostatic discharge/charge of $\text{Zn}|\text{LiOH}|\text{FePO}_4$ cell**

1 The FePO<sub>4</sub> active material was first mixed with 15 wt. % of carbon black (A-  
2 99, Asbury USA) and with 10 wt. % of poly(vinylidene difluoride) (PVDF, Sigma  
3 Aldrich) as a binder and then pressed into a disk shape with a diameter of 10 mm.  
4 Each disk was 0.5 mm thick and weighed approximately 35 mg. An electrochemical  
5 test cell was constructed with the disk as cathode, Zn metal as anode and filter paper  
6 (Whatman filters 12) as separator. The mass of zinc was at least ten times greater (to  
7 overcome the Zn depletion) than that required for a stoichiometric reaction between  
8 Zn and FePO<sub>4</sub>. The electrolyte was a 5 M of lithium hydroxide. Analytical reagent  
9 grade lithium hydroxide monohydrate (LiOH·H<sub>2</sub>O) and potassium hydroxide (KOH)  
10 were dissolved in de-ionized water to prepare solutions of the required concentrations.  
11 The cell was discharged/charged galvanostatically at 0.5 mA/cm<sup>2</sup> by using an 8  
12 channel battery analyser from MTI Corporation, USA, operated by a battery testing  
13 system (BTS).  
14  
15  
16  
17  
18  
19  
20  
21  
22  
23  
24  
25  
26  
27  
28  
29  
30

### 31 3. Results and Discussion

#### 32 3.1 Slow scan cyclic voltammetric investigation of FePO<sub>4</sub>

33 To study the reduction/oxidation mechanism of an FePO<sub>4</sub> cathode, slow scan cyclic  
34 voltammetry (CV) was used. In the CV technique, the potential determines the  
35 electrochemical reaction that occurs. The study involved slow scan CV in conjunction  
36 with the characterization of the materials formed during the electrochemical reduction  
37 and oxidation of FePO<sub>4</sub> by using various techniques i.e. XRD, SEM and XPS.  
38  
39  
40  
41  
42  
43  
44  
45  
46  
47  
48

49 The first and tenth cyclic voltammogram of FePO<sub>4</sub> in a LiOH aqueous  
50 electrolyte using Hg/HgO reference electrode is displayed in Fig. 1. The potential is  
51 displayed on the x-axis with potentials becoming more negative from right to left. A  
52 negative-going potential generates more strongly reducing conditions while a  
53 positive-going potential becomes more strongly oxidising. Current is shown on the y-  
54  
55  
56  
57  
58  
59  
60  
61  
62  
63  
64  
65

1 axis. A negative current corresponds to a reduction from  $\text{Fe}^{3+}$  to  $\text{Fe}^{2+}$  while a positive  
2 current is due to oxidation of  $\text{Fe}^{2+}$  to  $\text{Fe}^{3+}$ . At the potential where current is maximum  
3 is defined as a peak. The voltammogram consists of a reduction peak  $C_1$  at -275 mV  
4 and a corresponding anodic peak  $A_1$  at -12 mV. Figure 1 also shows the changes in  
5 CV profile when the material is subjected to continuous cycling (10 cycles) in the  
6 same potential region. In the tenth cycle, the cathodic and anodic peak current  
7 decreased to 85% and 10% (reducing the efficiency by 15% and 10%) respectively,  
8 however the material could be reversibly reduced/oxidised over multiple cycles. The  
9 observed reduction and oxidation potentials at -275 and -12 mV are less negative and  
10 positive than the hydrogen and oxygen evolution potentials that occur, suggesting that  
11  $\text{FePO}_4$  can be used as a cathode material in aqueous LiOH electrolyte.

12 In accordance with the objective of this work, the effect of replacing KOH  
13 with LiOH was determined by carrying out a cyclic voltammogram on two identical  
14 cells, one containing LiOH and the other KOH electrolyte. The behavior of  $\text{FePO}_4$  in  
15 aqueous LiOH cell can be compared to that in aqueous KOH by referring to Fig. 2.  
16 The CVs of  $\text{FePO}_4$  in the two electrolytes appear to be quite different. Two reduction  
17 peaks ( $C_1$  and  $C_2$ ) and an oxidation peaks ( $A_1$ ) are seen for the cell using KOH  
18 electrolyte, in the LiOH cell only one reduction ( $C_1$ ) and one oxidation peak ( $A_1$ ) are  
19 seen. Upon continuous cycling (in Fig. 3) in the same potential region as for KOH  
20 cell, the cathodic peak  $C_1$  disappears and the shape of the peak  $C_2$  is changed. The  
21 anodic peak  $A_1$  becomes more pronounced on cycling.

22 The redox potential observed for the LiOH cell is almost the same as values  
23 reported in the literature [10–13] for the non-aqueous electrolyte. Hence, this could  
24 correspond to a lithium intercalation/de-intercalation mechanism associated with the  
25  $\text{Fe}^{3+/2+}$  redox couple. While for the KOH cell, during an initial cycle,  $\text{K}^+$  ion insertion



1 is observed [19] as peak C<sub>1</sub>, but this process is not reversible after the 5<sup>th</sup> cycle in Fig.  
2  
3 3. The size of the K<sup>+</sup> ion (1.38 Å) is twice that of Li<sup>+</sup> (0.76 Å) in a VI-fold  
4 coordination [20] and hence the host trigonal structure is not stable for  
5 insertion/extraction of K<sup>+</sup> ions. Hence the cathodic peak C<sub>1</sub> corresponding to K<sup>+</sup>  
6 intercalation disappeared upon successive cycles. The peak C<sub>2</sub> corresponds to well-  
7 known proton insertion [21-22] into FePO<sub>4</sub> in aqueous KOH electrolyte which is  
8 reversible. Hence, unlike for Li<sup>+</sup>, the intercalation mechanism of K<sup>+</sup> is not reversible  
9 in the FePO<sub>4</sub> structure.  
10  
11  
12  
13  
14  
15  
16  
17

### 18 **3.2 Characterization of the FePO<sub>4</sub> cathode material**

19  
20  
21 The change in crystal structure after electro-reduction and electro-oxidation has been  
22 studied for the FePO<sub>4</sub> cathode by X-ray diffraction measurements as shown in Fig. 4.  
23  
24 The XRD pattern of the starting material (Fig. 4a) show that it is poorly crystalline  
25 and the tiny peaks are assigned to trigonal FePO<sub>4</sub> [23]. Figs. 4b and 4c show the XRD  
26 patterns of the material formed on scanning FePO<sub>4</sub> to C<sub>1</sub> (-275 mV) and A<sub>1</sub> (-12 mV)  
27 where reduction and oxidation occurs. The generation of new peaks in Fig. 4b match  
28 those reported in the literature [10, 24] and is in agreement with the simulated pattern  
29 shown (Fig. 4c) for lithium intercalated iron phosphate (LiFePO<sub>4</sub>), which indicates  
30 that LiFePO<sub>4</sub> is formed by the reduction of FePO<sub>4</sub>. This new material adopts an  
31 olivine structure of orthorhombic system [25] with intercalated lithium and iron  
32 cations located in octahedral sites. Thus the electro-reduction of FePO<sub>4</sub> in aqueous  
33 LiOH electrolyte involves the intercalation of Li<sup>+</sup> and hence the mechanism is quite  
34 similar to that reported in non-aqueous electrolyte. After the subsequent electro-  
35 oxidation, material formed in the oxidation cycle regenerates the original material.  
36  
37 The XRD pattern (Fig. 4d) of the regenerated material is almost identical to that of the  
38 original FePO<sub>4</sub> (in Fig. 4a) except for peaks at 2θ = 35.3 and 57 indicating the  
39  
40  
41  
42  
43  
44  
45  
46  
47  
48  
49  
50  
51  
52  
53  
54  
55  
56  
57  
58  
59  
60  
61  
62  
63  
64  
65

1 presence of LiFePO<sub>4</sub> material. The differences observed in the crystal structure from  
2 the delithiated phase of LiFePO<sub>4</sub> and trigonal FePO<sub>4</sub> are given in the literature [17].  
3

4  
5 The XRD pattern of the FePO<sub>4</sub> material formed after electro-reduction at -335  
6 mV and electro-oxidation at -14 mV in the KOH electrolyte is compared with the  
7 starting material in Fig. 5. The mechanism by which FePO<sub>4</sub> reduces is different from  
8 that of LiOH electrolyte. As can be seen from Fig. 5b, an evolution of new peaks is  
9 observed in the reduced material in addition to the parent compound. Clearly, these  
10 new peaks do not correspond to any of the lithium intercalated FePO<sub>4</sub>. However, these  
11 peaks are associated with the formation of the FeOOH (goethite) structure [26]. This  
12 suggests that the reduction mechanism of the FePO<sub>4</sub> cathode material is not the same  
13 as that observed for LiOH electrolyte. The XRD pattern (Fig. 5c) of the electro-  
14 oxidised material reverted back to the original material in addition to the formation of  
15 Fe<sub>2</sub>O<sub>3</sub> which is found to be not reversible.  
16  
17  
18  
19  
20  
21  
22  
23  
24  
25  
26  
27  
28  
29  
30

31 The surface morphologies of the FePO<sub>4</sub> cathode material formed after electro-  
32 reduction and electro-oxidation in LiOH and KOH electrolytes were determined by  
33 scanning electron microscopy. As can be seen from the micrograph, Fig. 6a, the  
34 morphology appears to be poorly crystalline as observed in the XRD spectra. The  
35 material formed after electro-reduction had a different morphology (Fig. 6b). A  
36 crystalline-like material of particle size 5-10 μm is observed, this could be a new  
37 phase (LiFePO<sub>4</sub>) generated by reduction. The subsequent oxidation of the reduced  
38 material (Fig. 6c) produced a phase (FePO<sub>4</sub>) whose morphology was quite similar to  
39 that of the original material. This was in contrast with the material (Fig. 7) formed  
40 after electro-reduction and oxidation of FePO<sub>4</sub> in the KOH cell. As evidenced by the  
41 XRD patterns (Fig. 5b-c), the observed morphology could be due to the formation of  
42  
43  
44  
45  
46  
47  
48  
49  
50  
51  
52  
53  
54  
55  
56  
57  
58  
59  
60  
61  
62  
63  
64  
65

1 iron oxy-hydroxide (FeOOH) during reduction and iron (III) oxide (Fe<sub>2</sub>O<sub>3</sub>) during  
2 subsequent oxidation that underwent an irreversible change during the cycle.  
3

4  
5 To confirm the presence of lithium ions in the electro-reduced/oxidised  
6 trigonal FePO<sub>4</sub> structure, an XPS analysis was carried out. Fig. 8 shows the XPS  
7 spectra of Li (1s) for the FePO<sub>4</sub> cathode. The material after electrochemical processes  
8 was found to be covered with a layer of Li<sub>2</sub>CO<sub>3</sub> been formed through the reaction of  
9 LiOH by the atmospheric CO<sub>2</sub>. This is not unexpected because the atmospheric CO<sub>2</sub> is  
10 not excluded from the experiment as the cell is not completely sealed. Hence, the  
11 material was washed thoroughly with acetone and de-ionised water several times until  
12 no further Li<sup>+</sup> ions were detected as indicated by the colour of the washings in the  
13 presence of phenolphthalein indicator. The washed material was mounted in the XPS  
14 analysis chamber and the spectra were recorded. It can be seen that the peak at 55.7  
15 eV, corresponding to Li, has a high intensity for electro-reduced but very low  
16 intensity for electro-oxidised sample. This low in intensity peak confirms that a small  
17 amount of lithium associated with FePO<sub>4</sub> is still present even after oxidation, as what  
18 seen in the XRD pattern of Fig. 4d. From the evidence of XRD and XPS studies, it  
19 can be concluded that lithium is intercalated into the host FePO<sub>4</sub> when aqueous LiOH  
20 is the electrolyte. The mechanism is found to be reversible.  
21  
22  
23  
24  
25  
26  
27  
28  
29  
30  
31  
32  
33  
34  
35  
36  
37  
38  
39  
40  
41  
42

### 43 ***3.3. Galvanostatic discharge-charge of FePO<sub>4</sub> in LiOH electrolyte***

44  
45 The Zn|LiOH|FePO<sub>4</sub> cell was discharged and charged galvanostatically at 0.5 mA/cm<sup>2</sup>  
46 using a battery analyser. A typical discharge-charge curve of the aqueous cell is  
47 shown in Fig. 9. The initial open-circuit voltage was around 1.0 V. On discharge, the  
48 cell voltage fell at a constant rate to 0.4 V corresponding to 60 mAh/g and then  
49 decreased sharply to a cut-off voltage of 0.2 V. The overall discharge capacity is  
50 calculated to be 65 mAh/g. Upon charging the material at constant current, the voltage  
51  
52  
53  
54  
55  
56  
57  
58  
59  
60  
61  
62  
63  
64  
65

1 increased steeply to 1.4 V corresponding to 40 mAh/g and then the voltage gradually  
2 increased to a cut-off voltage of 1.6 V. The charge capacity is fully reversible, as  
3 reflected in the cyclic voltammetry (Fig. 1) experiment that the  $\text{Fe}^{3+}/^{2+}$  redox couple is  
4 fully accessible for amorphous  $\text{FePO}_4$  material. Thus, within the operating voltage  
5 window maximum capacity was derived from the  $\text{FePO}_4$  material. The cycleability of  
6 the  $\text{FePO}_4$  battery has been examined and it was found that cycleability retention  
7 wasn't very attractive to be suitable for energy storage applications. This could be due  
8 to the formation non-rechargeable products which are inevitable in aqueous solutions.  
9 However, these products could be suppressed by adding suitable additives [15-16] to  
10 the  $\text{FePO}_4$  cathode to enhance the performance. Trigonal  $\text{FePO}_4$  might be a potential  
11 cathode material for an aqueous battery system provided its stability in alkaline  
12 electrolyte and electrochemical properties are improved.

#### 29 4. Conclusions

31 Lithium intercalation into a  $\text{FePO}_4$  cathode in an aqueous electrolyte has been  
32 investigated. Cyclic voltammetry results show that  $\text{FePO}_4$  undergoes a reversible  
33 ( $\text{Fe}^{3+}/\text{Fe}^{2+}$ ) process of reduction and oxidation in lithium hydroxide electrolyte. X-ray  
34 diffraction of the reduced and oxidised  $\text{FePO}_4$  shows that the process undergoes a  
35 lithium intercalation and de-intercalation mechanism to form  $\text{LiFePO}_4$  and  $\text{FePO}_4$ . An  
36 X-ray photoelectron spectroscopy study confirms the presence of lithium in the solid  
37 matrix of the  $\text{FePO}_4$  cathode. Whereas, using KOH electrolyte, intercalation of the  
38 potassium ion ( $\text{K}^+$ ) is associated with proton intercalation during reduction.  $\text{K}^+$  ion  
39 intercalation is found to be irreversible in the successive cycles. The discharge  
40 capacity of the  $\text{Zn}|\text{LiOH}|\text{FePO}_4$  battery was calculated to be 65 mAh/g. The discharge  
41 voltage of this battery needs to be improved to compete with well-established non-  
42 aqueous counterparts. Nevertheless, this material is an interesting alternative for  
43  
44  
45  
46  
47  
48  
49  
50  
51  
52  
53  
54  
55  
56  
57  
58  
59  
60  
61  
62  
63  
64  
65

1 lithium intercalation in terms of low cost, environmental friendliness and safety  
2 issues.  
3

#### 4 Acknowledgement 5

6  
7 The author wishes to acknowledge the Australian Research Council (ARC). This  
8 article was produced as an outcome of the ARC Discovery Project grant  
9 (DP1092543).  
10  
11  
12  
13

#### 14 References 15

- 16  
17 [1] M. S. Whittingham, *Chem. Rev.* **104** (2004) 4271.  
18  
19 [2] Y. Shin and A. Manthiram, *Electrochem. Solid State Lett.* **5(3)** (2002) A55.  
20  
21 [3] A. K. Padhi, K.S. Nanjundaswamy, C. Masquelier, S. Okada and J. B.  
22 Goodenough, *J. Electrochem. Soc.* **144** (1997) 1609.  
23  
24 [4] K. Konstantinov, S. Bewlay, G. X. Wang, M. Lindsay, J.Z. Wang, H.K. Liu, S.X.  
25 Dou and J.-H. Ahn, *Electrochim. Acta* **50** (2004) 421.  
26  
27 [5] C. H. Mi, G.S. Cao and X.B. Zhao, *Mater. Lett.* **59** (2005) 127.  
28  
29 [6] B. Wang, Y. Qiu and S. Ni, *Solid State Ionics* **178** (2007) 843.  
30  
31 [7] F. Yu, J. Zhang, Y. Yang and G. Song, *Electrochim. Acta* **54** (2009) 7389.  
32  
33 [8] X. Gao, G. Hu, Z. Peng and K. Du, *Electrochim. Acta* **54** (2009) 4777.  
34  
35 [9] H. Okawa, J. Yabuki, Y. Kawamura, I. Arise and M. Sato, *Mat. Res. Bull.* **43**  
36 (2008) 1203.  
37  
38 [10] A.K. Padhi, K.S. Nanjundaswamy and J. B. Goodenough, *J. Electrochem. Soc.*  
39 144 (1997) 1188.  
40  
41 [11] C.V. Ramana, A. Mauger, F. Gendron, C. M. Julien and K. Zaghib, *J. Power*  
42 Sources **187** (2009) 555.  
43  
44 [12] N. Kalaiselvi and A. Manthiram, *J. Power Sources* **195** (2010) 2894.  
45  
46  
47  
48  
49  
50  
51  
52  
53  
54  
55  
56  
57  
58  
59  
60  
61  
62  
63  
64  
65

- 1  
2  
3  
4  
5  
6  
7  
8  
9  
10  
11  
12  
13  
14  
15  
16  
17  
18  
19  
20  
21  
22  
23  
24  
25  
26  
27  
28  
29  
30  
31  
32  
33  
34  
35  
36  
37  
38  
39  
40  
41  
42  
43  
44  
45  
46  
47  
48  
49  
50  
51  
52  
53  
54  
55
- [13] J. Molenda, W. Ojczyk, K. Swierczek, W. Zajac, F. Krok, J. Dygas and R. Liu, Solid State Ionics **177** (2006) 2617.
- [14] M. Minakshi, P. Singh, T.B. Issa, S. Thurgate and R. DeMarco, J. Power Sources **130** (2004) 254.
- [15] M. Minakshi and D. R. G. Mitchell, Electrochim. Acta **53** (2008) 6323.
- [16] M. Minakshi, D. R. G. Mitchell and P. Singh, Electrochim. Acta **52** (2007) 3294.
- [17] S. Okada, T. Yamamoto, Y. Okazaki, J. Yamaki, M. Tokunaga and T. Nishida, J. Power Sources **146** (2005) 570.
- [18] Y. Song, S. Yang, P.Y. Zavalij and M.S. Whittingham, Mat. Res. Bull. **37** (2002) 1249.
- [19] M. Minakshi, J. Electroanal. Chem. **616** (2008) 99.
- [20] R.D. Shannon, Acta. Crystallogr. A **32** (1976) 751.
- [21] H. Schlorb, M. Bungs and W. Plieth, Electrochim. Acta **42** (1996) 2619.
- [22] K. S. Abou-El-Sherbini and M. H. Askar, J. Solid State Electrochem. **7** (2003) 435.
- [23] International Centre for Diffraction Data No. 29-0715.
- [24] M. Minakshi, P. Singh, T. B. Issa, S. Thurgate, and K. Prince, Key Engineering Materials, **320** (2006) 271.
- [25] K. F. Hsu, S. K. Hu, C. H. Chen, M. Y. Cheng, S. Y. Tsay, T. C. Chou, H. S. Sheu, J. F. Lee and B. J. Hwang, J. Power Sources **192** (2009) 660.
- [26] International Centre for Diffraction Data No. 44-1415.

### **Figure Captions**

56  
57  
58  
59  
60  
61  
62  
63  
64  
65

**Fig. 1** A typical cyclic voltammogram of iron phosphate ( $\text{FePO}_4$ ) in aqueous lithium hydroxide electrolyte (scan rate:  $25 \mu\text{V} \cdot \text{s}^{-1}$ ; potential limit: 0.2 to -0.4 V and back). Cycle numbers are indicated in the figure.

1  
2  
3  
4  
5  
6  
7  
8  
9  
10  
11  
12  
13  
14  
15  
16  
17  
18  
19  
20  
21  
22  
23  
24  
25  
26  
27  
28  
29  
30  
31  
32  
33  
34  
35  
36  
37  
38  
39  
40  
41  
42  
43  
44  
45  
46  
47  
48  
49  
50  
51  
52  
53  
54  
55  
56  
57  
58  
59  
60  
61  
62  
63  
64  
65

**Fig. 2** Cyclic voltammogram of FePO<sub>4</sub> in aqueous lithium hydroxide and potassium hydroxide electrolytes for the first cycle. The potential scanned at 25 μV. s<sup>-1</sup> from 0.2 to -0.4 V and back.

**Fig. 3** Cyclic voltammogram of FePO<sub>4</sub> in aqueous potassium hydroxide electrolyte for the repeated cycles, potential scanned at 25 μV. s<sup>-1</sup> from 0.2 to -0.4 V and back. The numbers in figures denoted cycle number.

**Fig. 4** X-ray diffraction patterns of FePO<sub>4</sub> (a) before electro reduction (b) after the first cycle of electro reduction at -275 mV (c) simulated pattern of LiFePO<sub>4</sub>: orthorhombic – olivine like structure (PNMA space group) and (d) after subsequent electro oxidation at -12 mV in aqueous LiOH electrolyte.

**Fig. 5** X-ray diffraction patterns of FePO<sub>4</sub> (a) before electro reduction (b) after the first cycle of electro reduction at -335 mV and (c) after subsequent electro oxidation at -14 mV in aqueous KOH electrolyte.

**Fig. 6** Scanning electron images of FePO<sub>4</sub> (a) before electro reduction (b) after the first cycle of electro reduction and (c) after subsequent electro oxidation in aqueous LiOH electrolyte.

**Fig. 7** Scanning electron images of FePO<sub>4</sub> (a) after the first cycle of electro reduction and (b) after subsequent electro oxidation in aqueous KOH electrolyte.

**Fig. 8** XPS spectra of Li 1s of FePO<sub>4</sub> (a) after the first cycle of electro reduction and (b) after subsequent electro oxidation in aqueous LiOH electrolyte.

**Fig. 9** First (Galvanostatic) discharge-charge cycle of Zn-FePO<sub>4</sub> cell using aqueous LiOH electrolyte.

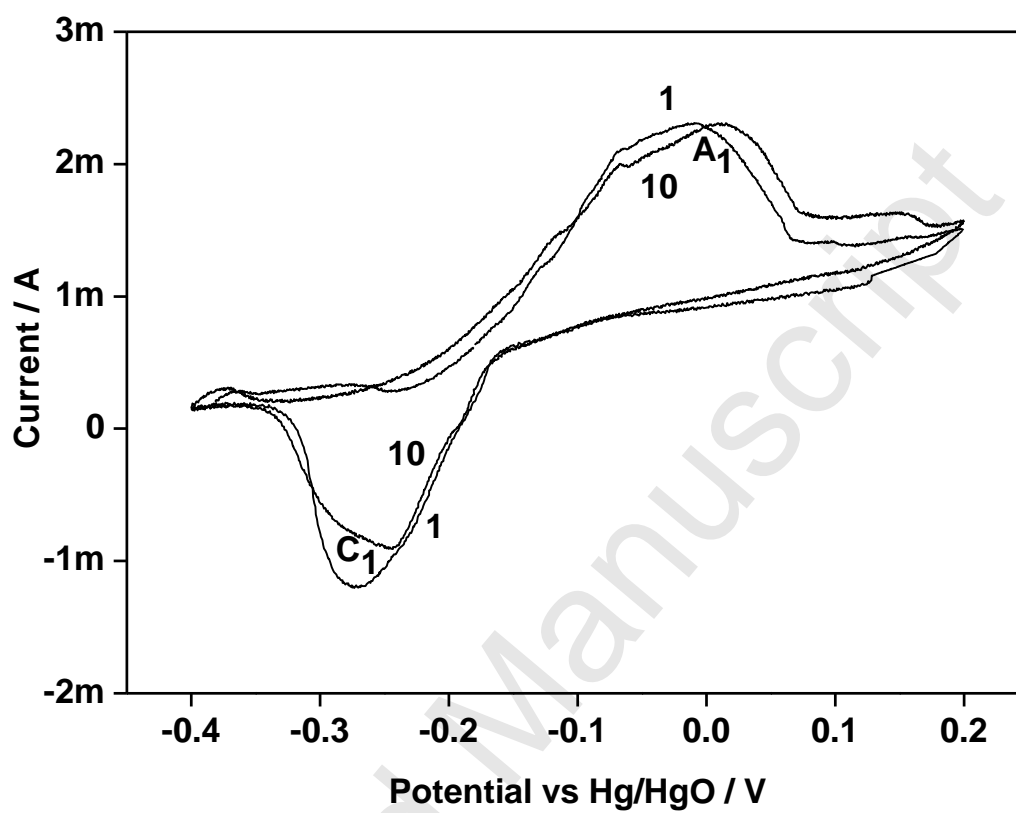


**Fig. 1** A typical cyclic voltammogram of iron phosphate ( $\text{FePO}_4$ ) in aqueous lithium hydroxide electrolyte (scan rate:  $25 \mu\text{V} \cdot \text{s}^{-1}$ ; potential limit: 0.2 to -0.4 V and back). Cycle numbers are indicated in the figure.



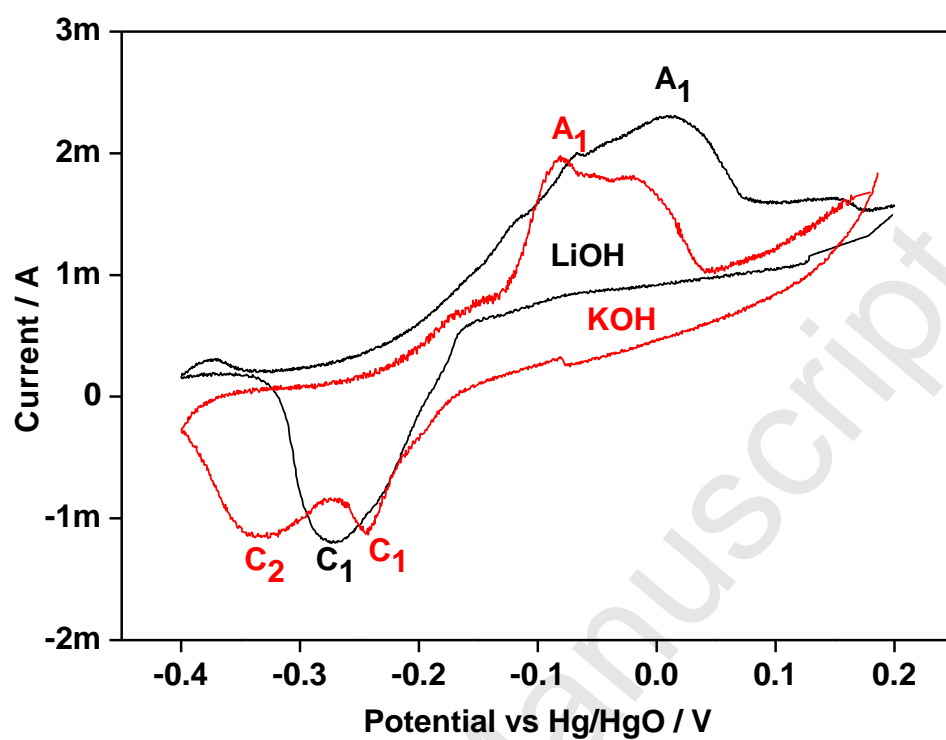


**Fig. 2** Cyclic voltammogram of FePO<sub>4</sub> in aqueous lithium hydroxide and potassium hydroxide electrolytes for the first cycle. The potential scanned at 25  $\mu\text{V} \cdot \text{s}^{-1}$  from 0.2 to -0.4 V and back.

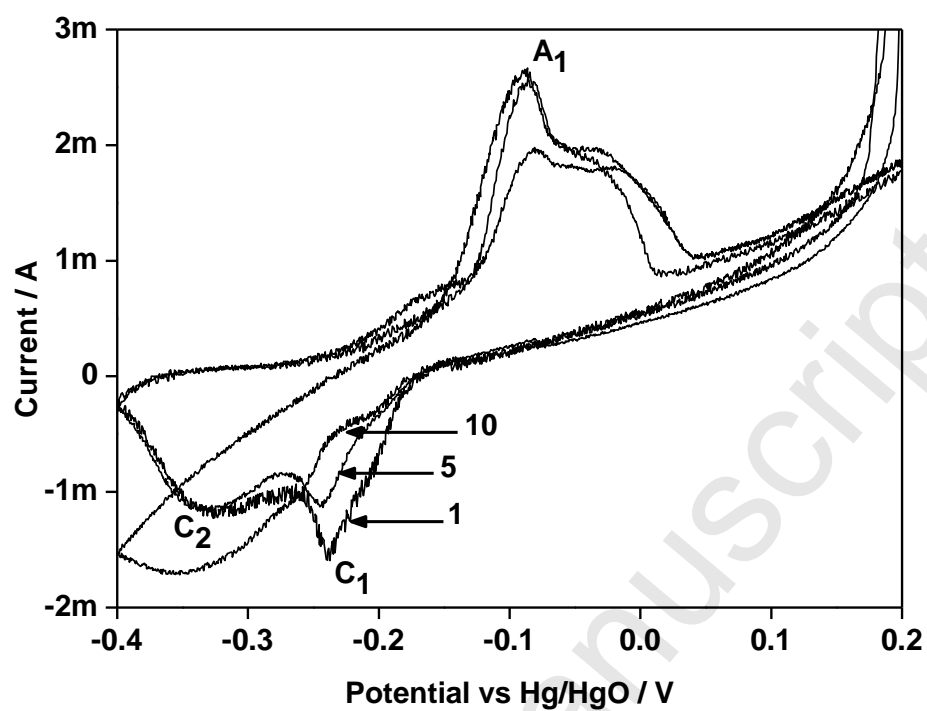


**Fig. 3** Cyclic voltammogram of  $\text{FePO}_4$  in aqueous potassium hydroxide electrolyte for the repeated cycles, potential scanned at  $25 \mu\text{V} \cdot \text{s}^{-1}$  from 0.2 to -0.4 V and back. The numbers in figures denoted cycle number.

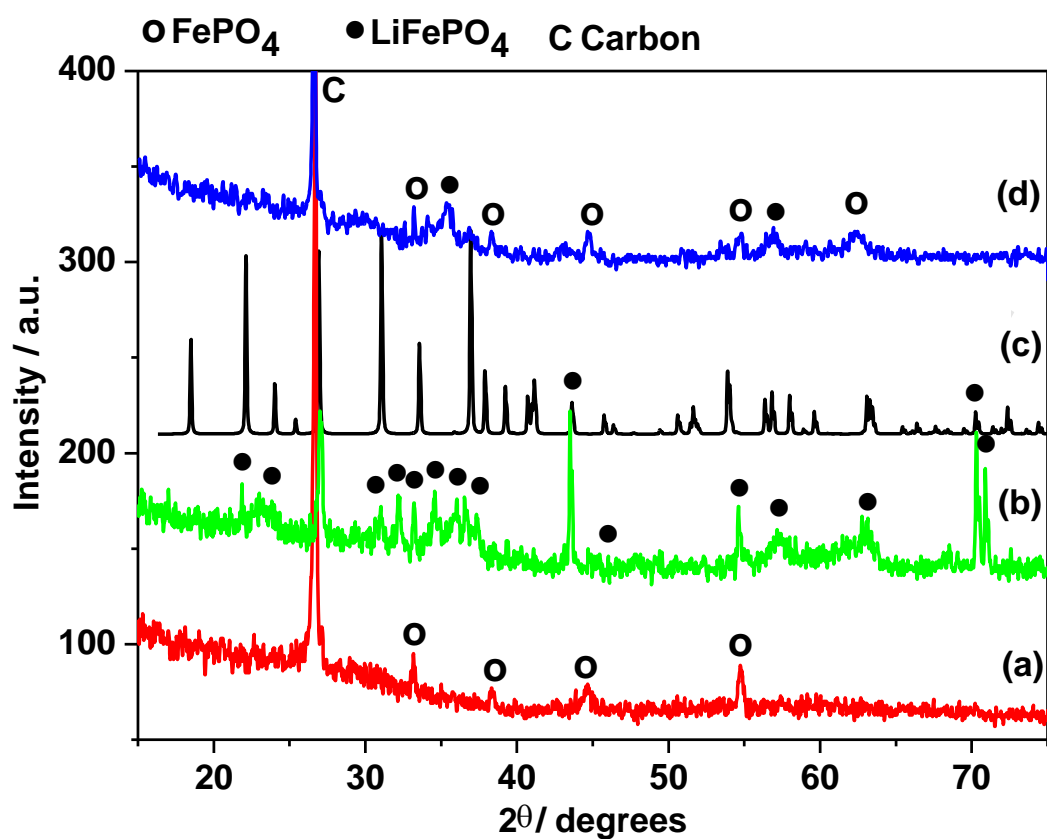


**Fig. 4** X-ray diffraction patterns of  $\text{FePO}_4$  (a) before electro reduction (b) after the first cycle of electro reduction at  $-275$  mV (c) simulated pattern of  $\text{LiFePO}_4$ : orthorhombic – olivine like structure (PNMA space group) and (d) after subsequent electro oxidation at  $-12$  mV in aqueous  $\text{LiOH}$  electrolyte.

ACCEPTED

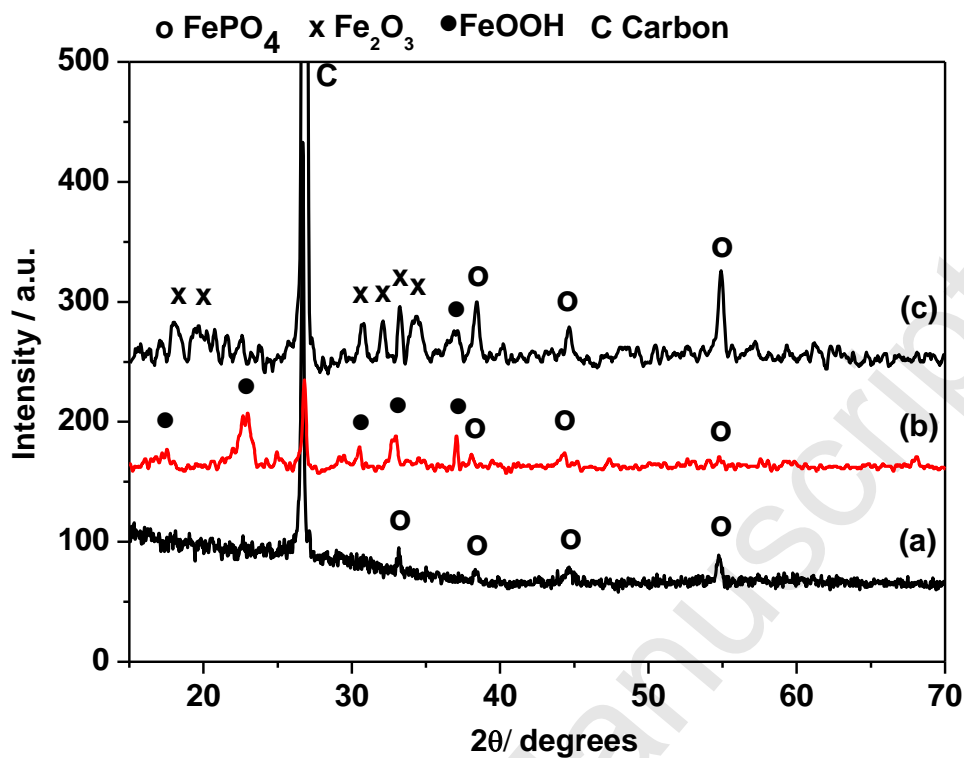


**Fig. 5** X-ray diffraction patterns of FePO<sub>4</sub> (a) before electro reduction (b) after the first cycle of electro reduction at -335 mV and (c) after subsequent electro oxidation at -14 mV in aqueous KOH electrolyte.

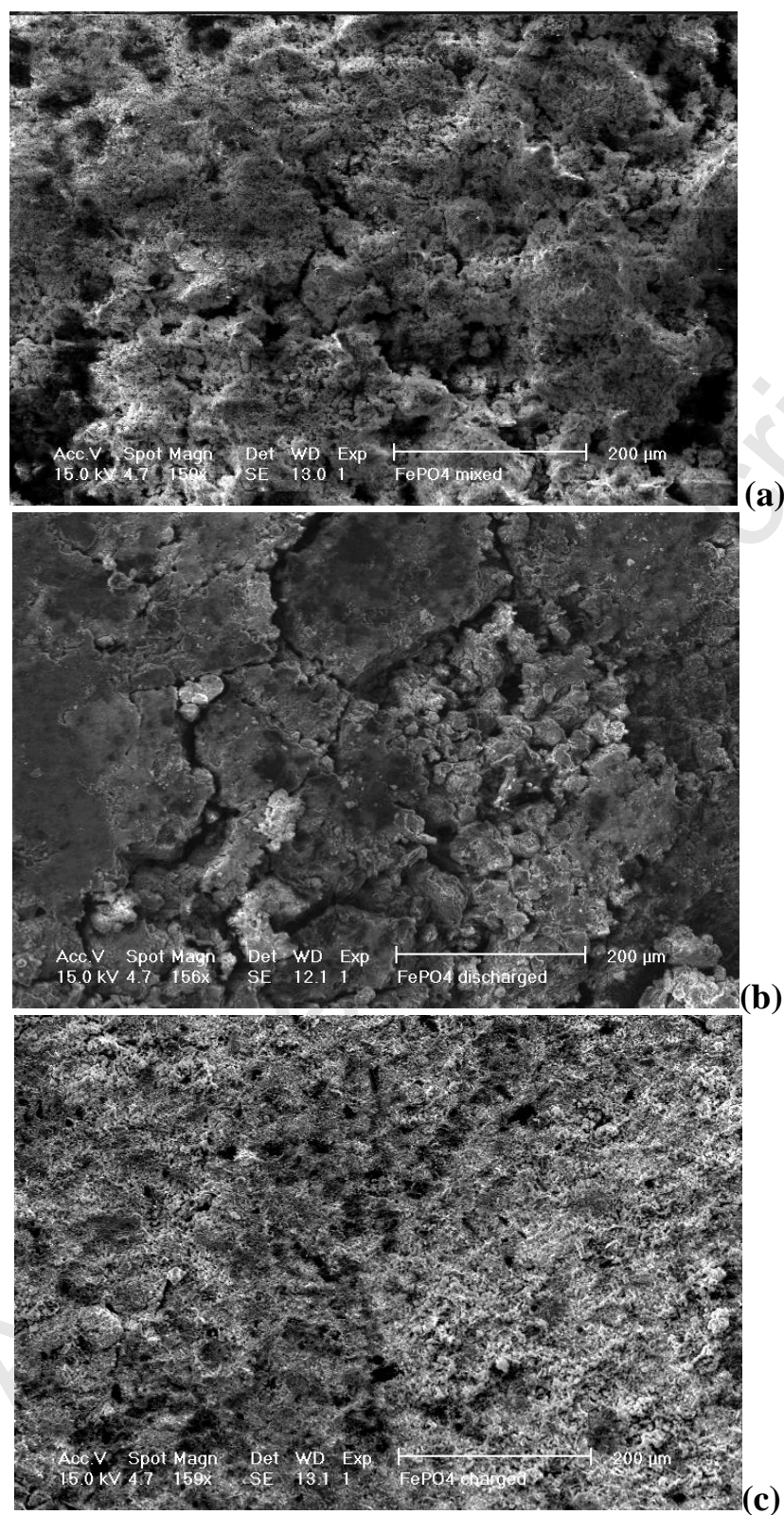


**Fig. 6** Scanning electron images of FePO<sub>4</sub> (a) before electro reduction (b) after the first cycle of electro reduction and (c) after subsequent electro oxidation in aqueous LiOH electrolyte.

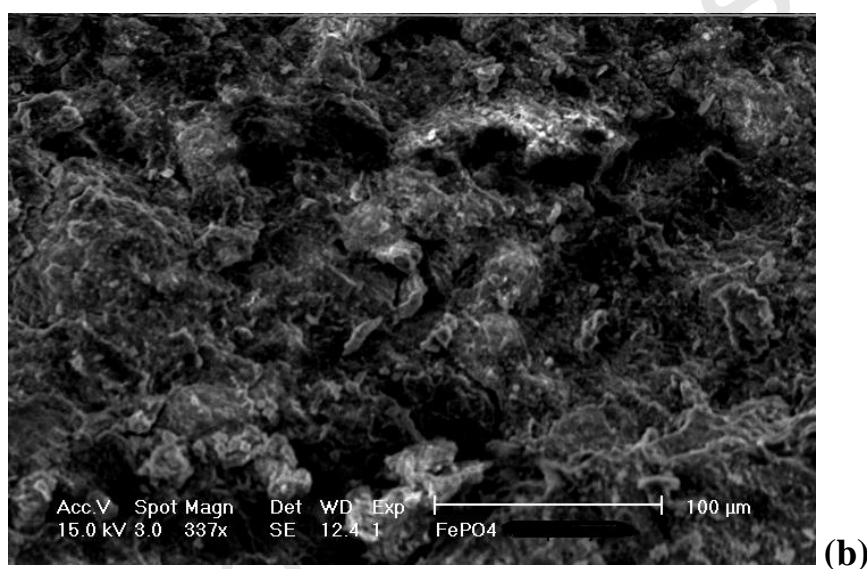
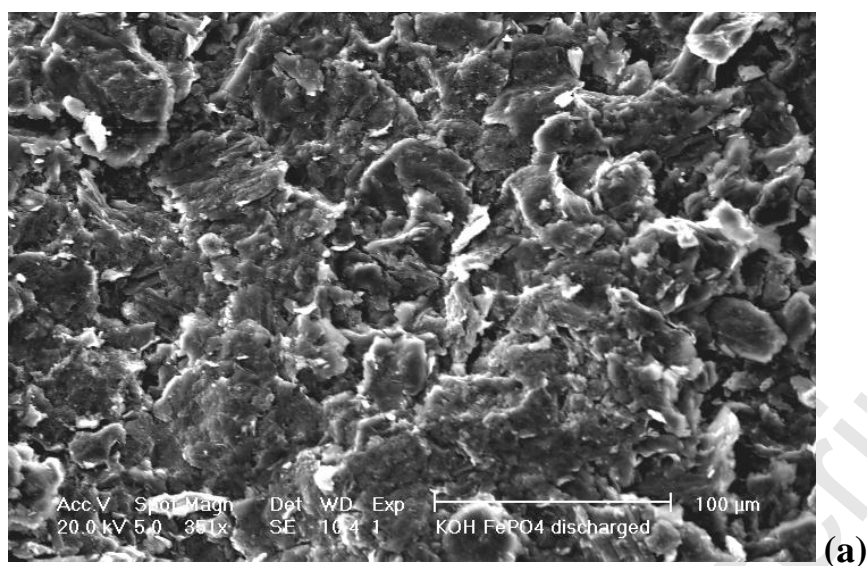


**Fig. 7** Scanning electron images of FePO<sub>4</sub> (a) after the first cycle of electro reduction and (b) after subsequent electro oxidation in aqueous KOH electrolyte.

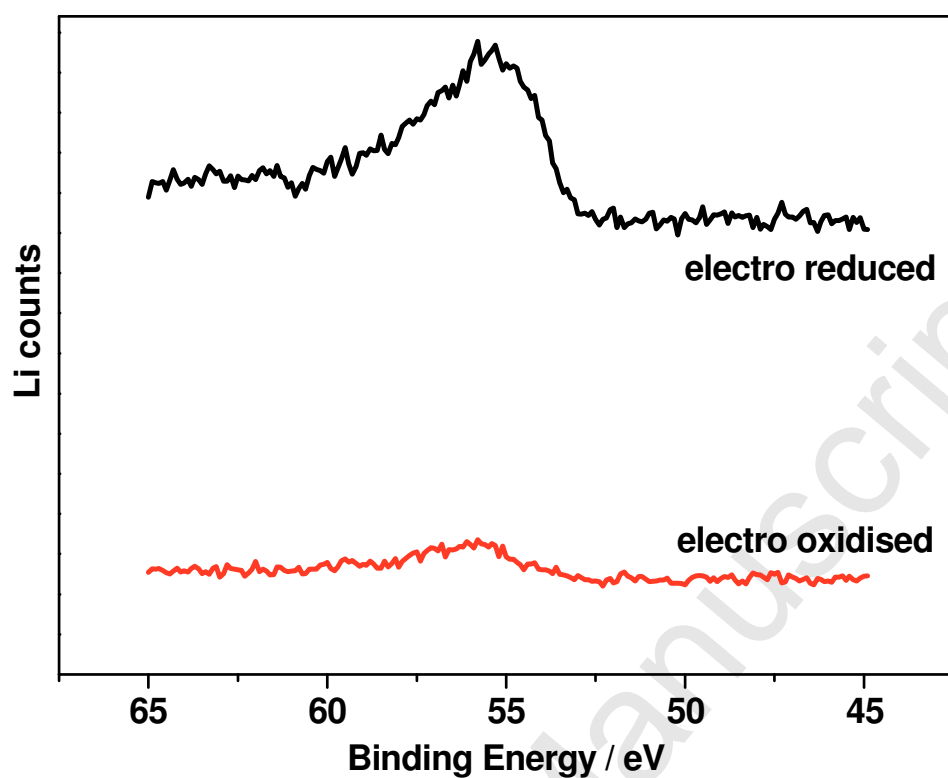


**Fig. 8** XPS spectra of Li 1s of FePO<sub>4</sub> (a) after the first cycle of electro reduction and (b) after subsequent electro oxidation in aqueous LiOH electrolyte.

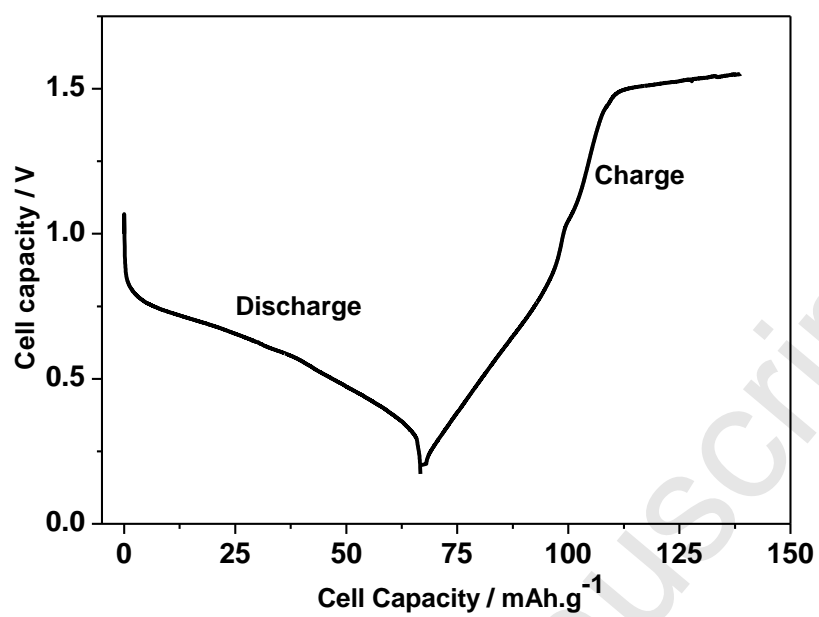


**Fig. 9** First (Galvanostatic) discharge-charge cycle of Zn-FePO<sub>4</sub> cell using aqueous LiOH electrolyte.